Theory and Observations of Controls on Lightning Flash Size Spectra

ERIC C. BRUNING

Texas Tech University, Lubbock, Texas

DONALD R. MACGORMAN

National Severe Storms Laboratory, Norman, Oklahoma

(Manuscript received 18 October 2012, in final form 26 July 2013)

ABSTRACT

Previous analyses of very high frequency (VHF) Lightning Mapping Array (LMA) observations relative to the location of deep convective updrafts have noted a systematic pattern in flash characteristics. In and near strong updrafts, flashes tend to be smaller and more frequent, while flashes far from strong vertical drafts exhibit the opposite tendency. This study quantitatively tests these past anecdotal observations using LMA data for two supercell storms that occurred in Oklahoma in 2004. The data support a prediction from electrostatics that frequent breakdown and large flash extents are opposed. An energetic scaling that combines flash rate and flash area exhibits a $^{5}/_{3}$ power-law scaling regime on scales of a few kilometers and a maximum in flash energy at about 10 km. The spectral shape is surprisingly consistent across a range of moderate to large flash rates. The shape of this lightning flash energy spectrum is similar to that expected of turbulent kinetic energy spectra in thunderstorms. In line with the hypothesized role of convective motions as the generator of thunderstorm electrical energy, the correspondence between kinematic and electrical energy spectra suggests that advection of charge-bearing precipitation by the storm's flow, including in turbulent eddies, couples the electrical and kinematic properties of a thunderstorm.

1. Introduction

This study is concerned with the following simple, fundamental questions:

(i) Where does lightning start?
(ii) Where does lightning go?
(iii) What do lightning data tell us about thunderstorm energetics?

Questions (i) and (ii) have seen significant advancement in the past decade with the advent of readily available data from very high frequency (VHF) Lightning Mapping Arrays (LMAs; Krehbiel et al. 2000; Thomas et al. 2004). LMAs map lightning channels in the cloud with sufficient time resolution and spatial precision to locate the origin and propagation of each flash throughout a storm's life cycle. The temporal and spatial resolution of LMA data makes it trivial to analyze patterns in the individual flashes relative to storm characteristics indicated by satellite and radar data. Charge structures inferred from LMAs in the Severe Thunderstorm Electrification and Precipitation Study (STEPS; Lang et al. 2004) and Thunderstorm Electrification and Lightning Experiment (TELEX; MacGorman et al. 2008) field programs have been essential in assessing conditions that support positive or negative ground and cloud flashes and the storm-relative locations in which those flashes happen.

The energy dissipated by lightning flashes [question (iii)] is extracted from a combination of gravitational potential and convective action (Braham 1952, 1953; Williams 1985; Weinheimer 1987). In both cases, a force must act over some distance on charged hydrometeors and against the net electric field to produce a net potential reservoir. The work of interest to electrification is, to a very good approximation, positional. In the case of gravity, work depends on an object's location relative approximately to Earth's center of mass, while in the case of electrical energy it depends on the instantaneous location of all the charges creating the electric field.

Corresponding author address: Eric C. Bruning, Texas Tech University, Department of Geosciences, Atmospheric Science Group, Texas Tech University, Box 41053, Lubbock, TX 79409.
E-mail: eric.bruning@ttu.edu

DOI: 10.1175/JAS-D-12-0289.1

One of the challenging questions posed here is the extent to which the electrical and kinematic systems are coupled. A number of papers have been published (e.g., Rust et al. 1982; Ray et al. 1987; Carey et al. 2005; Tessendorf et al. 2005; Wiens et al. 2005; Tessendorf et al. 2007; Ely et al. 2008; Bruning et al. 2007; Lund et al. 2009; Bruning et al. 2010; Emersic et al. 2011; Calhoun et al. 2013) that relate VHF lightning mapping data to kinematic structure and precipitation trajectories in mesoscale convective systems, supercells, and ordinary ''airmass'' thunderstorms. A close correspondence has been found between deep convective cells and high flash rates, with lower flash rates in advected ice-phase clouds downshear from the convective cores [these principles underlie the McCaul et al. (2009) lightning parameterization]. Many of these authors have noted that flashes near deep convective updrafts are generally smaller in size, while flashes in stratiform or anvil regions tend to have large extents (Carey et al. 2005; Kuhlman et al. 2009; Weiss et al. 2012). This study investigates these anecdotal observations by examining local and whole-storm characteristics of the flash energy spectrum and associated implications for the distribution of electrostatic quantities within thunderstorms.

2. Electrostatic conditions for channel development

The following are basic electrostatic equations defining the relationships among the vector electric field **E**, the potential ϕ, and charge density ρ:

$$\mathbf{E} = -\nabla\phi; \tag{1}$$

$$\rho = \epsilon_0 \nabla \cdot \mathbf{E}; \tag{2}$$

and the corresponding relationship between charge density and potential,

$$\rho = -\epsilon_0 \nabla^2 \phi, \tag{3}$$

where ϵ_0 is the permittivity of air.

a. Initial breakdown

An extensive lightning channel tree begins with breakdown of the air in or near a local extremum in electric field in excess of some threshold (MacGorman et al. 1981, 2001; Maggio et al. 2005; Marshall et al. 2005; Stolzenburg et al. 2007).

A large electric field necessarily implies

$$\nabla\phi \neq 0. \tag{4}$$

The condition for the extremum is

$$\nabla \cdot \mathbf{E} = 0, \tag{5}$$

$$\nabla^2 \mathbf{E} \neq 0. \tag{6}$$

Substituting Eqs. (1) and (2) makes the maximization criteria

$$\rho = 0, \tag{7}$$

$$\nabla\rho \neq 0. \tag{8}$$

b. Extent

After initiation, the lightning channel grows bidirectionally (Kasemir 1960; Mazur and Ruhnke 1993; Mazur 2002). Each end of the lightning flash tends to propagate toward and then remain within a potential well about an extremum in potential (MacGorman et al. 2001; Coleman et al. 2003). There is some equipotential surface that defines the boundary of the well and acts as the upper limit on the spatial extent of that end of the flash. Extrema in potential are given by

$$\nabla\phi = 0, \tag{9}$$

$$\nabla^2 \phi \neq 0. \tag{10}$$

Substituting from Eqs. (1) and (2),

$$\mathbf{E} = 0, \tag{11}$$

$$\rho \neq 0. \tag{12}$$

Thus, extrema in potential occur within regions of charge, and one would expect that, after a flash is initiated, much of the propagation at each end of a flash would tend to remain within regions of charge and to reflect the geometry of those regions, as suggested by MacGorman et al. (1981) and Williams et al. (1985) based on observations of lightning and sparks, respectively.

The channel growth process itself requires a large electric field at the channel tip to continue. However, as a channel tip approaches a minimum in the potential, the ambient **E** provided by the storm's charge distribution becomes small there, as indicated by Eq. (11). Thus, if the channel is to extend farther, the electric field produced by the channel itself must cause the local **E** at the tip to exceed the threshold for continued propagation (MacGorman et al. 2001). Because the lightning channel is an excellent electrical conductor that can be approximated as having an equipotential surface, it is the difference between the potential of the channel and the local ambient potential that controls whether propagation can continue (Mazur 2002; Mansell et al. 2002). As

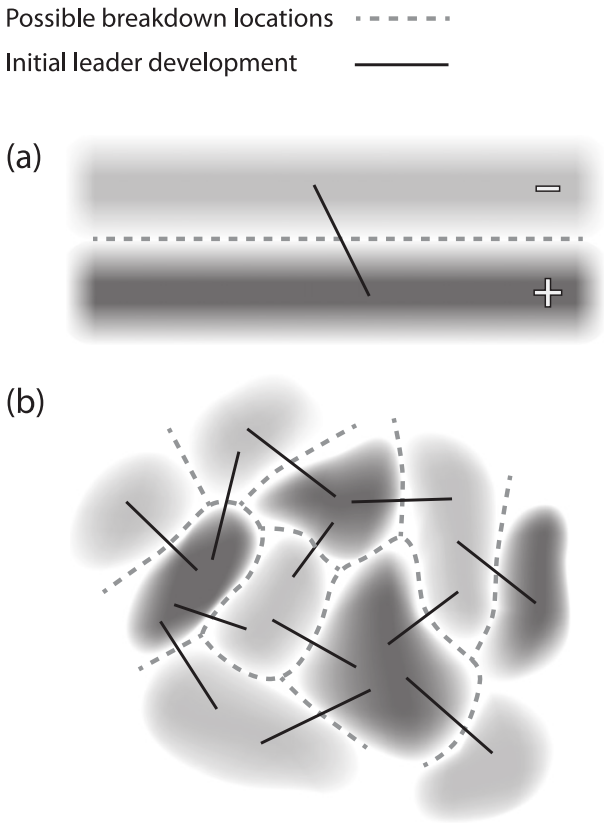

FIG. 1. Two idealized charge structures showing (a) extensive, horizontally stratified charge and (b) smaller pockets or blobs of charge. Dark gray blobs or regions are positive charge, while lighter gray is negative charge. Dashed gray lines indicate regions of large electric field where breakdown might begin. Solid black lines indicate where leaders would develop and propagate toward the center of the charge regions after initial breakdown.

the channel grows, eventually it will reach a point at which the magnitude of **E** due to this difference in potential decreases below the threshold for continued propagation, and the growth in that direction will stop (MacGorman et al. 2001; Mansell et al. 2002).

c. *Breakdown and extent are opposed*

Comparing Eq. (7) with Eq. (12) and Eq. (4) with Eq. (9) shows that the conditions for breakdown and extensive propagation are opposed. This opposition extends to the nature of flashes supported by a given charging rate. To see this, consider the positive and negative charge regions between which a flash initiates and through which it propagates.

Geometries permitting extensive horizontal propagation of lightning channels through the two charge regions after initiation, such as the extensive horizontal regions of weak **E** and constant ϕ in smooth, layered charge distributions (Fig. 1a), require more charge in each of the two oppositely charged regions to create **E** magnitudes large enough for breakdown than is the case for geometries having two (or more) small charge regions (Fig. 1b). Thus, a given storm charging rate can support larger flash rates for small flashes than for flashes involving large horizontal areas. Additionally, many small adjacent regions of alternating sign in charge provide many sites at which the potential gradient is locally at a maximum. Together, this suggests that flash rates and average flash areas can be used as local measures for the opposing conditions required for breakdown and spatial extent. Specifically, small flashes would be expected in regions having large flash initiation rates, and vice versa.

Note, however, that to produce **E** sufficient for breakdown, the two small charge regions must be closer together than is necessary for two smooth, layered charge regions, and large magnitudes of **E** necessarily extend over a much larger volume for smooth, extensive distributions than for small localized distributions. Because the energy required to create the charge regions is proportional to the volume integral of $|\mathbf{E}|^2$ produced by the charge, it requires much more energy to support each horizontally extensive flash.

A Fourier analysis shows that extrema in electrical potential are also extrema in charge. The potential field along a given direction x can be written as the sum of Fourier components

$$\phi = \sum_k a_k \sin(kx) = \sum_k F_k, \tag{13}$$

with amplitude a_k for wavenumber k. Applying Eq. (3) to get a Fourier series for charge density gives

$$\rho_k = \epsilon_0 a_k k^2 \sin(kx) = k^2 F_k \tag{14}$$

for each term, which has the same factor and phase dependence but amplifies the influence of large-wavenumber (small wavelength) components. Therefore, one may reason in terms of potential or charge density—whatever is convenient for the situation. (Meteorologists will recognize this methodology from diagnosis of the quasigeostrophic omega equation for vertical motion.) Using this principle, we can infer that the condition for channel propagation is that charge density or potential gradients are bounded along the direction of channel propagation at least enough to prevent a change in charge polarity.

While the texture of charge regions in real thunderstorms has not been a major theme in the literature, there is some evidence from in situ measurements that

charge is not purely layered. In particular, the vector electric field measurements in Mo et al. (2002), MacGorman et al. (2005), and Rust et al. (2005) show variability down to the scale of a kilometer in some cases. Stolzenburg and Marshall (1994) required at least some horizontal variability in their charge models to reproduce observed values of the horizontal field.

d. Energetic dimensional analysis

To characterize flash energetics we use dimensional arguments and the principles outlined above to derive a dimensional combination of flash observables that corresponds to the electrostatic conditions that control flash size and extent. The target energetic quantity is specific energy ($\mathrm{J\,kg^{-1}}$).

Denote flash area A as a measure of the flash extent within a net potential well. Denote flash rate η. Brackets denote the unit operator. The count (No.) part of flash rate is unitless. A dimensional combination for specific energy using flash area and flash rate is given by

$$[A] = \mathrm{m}^2, \tag{15}$$

$$[\eta] = \mathrm{No.\,s^{-1}}, \tag{16}$$

$$[A\eta^2] = \mathrm{m^2\,s^{-2}} = \mathrm{J\,kg^{-1}}. \tag{17}$$

From purely dimensional reasoning, a length scale l may be defined as

$$[l] = [\sqrt{A}] = \mathrm{m}. \tag{18}$$

Calculation of l as the square root of the flash area makes the assumption that the macroscale potential wells discharged by each flash are roughly planar and axisymmetric. The axisymmetric assumption was also made by Stolzenburg and Marshall (1994), who examined the impact of the variation in the diameter of the charged disks on electrostatic measurements within thunderstorms. This length scale should not be confused with the microscale channel length that accounts for the tortuous propagation of lightning's many branches.

The dimensional combination above may be interpreted by considering the energy dissipated by the discharge of a plane-parallel capacitor with charged plate area A and separation d. It may be shown that the energy U dissipated when a capacitor discharges at a breakdown field of E_b is

$$U = \frac{\epsilon_0}{2} E_b^2 A d. \tag{19}$$

It is apparent that the energy dissipated by the capacitor's discharge (which may be interpreted as a flash) is proportional to both A and d. Therefore, it constitutes a simplification to consider only the flash area and not its volume. It will be shown that this simplification still results in repeatable patterns in the storm's electrical energy spectrum.

The units for electric potential are

$$[\phi] = \mathrm{J\,C^{-1}} = \mathrm{V}. \tag{20}$$

Charge density ρ_q and volume V may be used to write

$$[\rho] = \mathrm{C\,m^{-3}}, \tag{21}$$

$$[\phi\rho V] = \mathrm{J}. \tag{22}$$

Or in terms of specific energy, and denoting ρ_a as the (mass) density of air:

$$\left[\phi\frac{\rho}{\rho_a}\right] = [A\eta^2] = [(l\eta)^2] = \mathrm{J\,kg^{-1}}. \tag{23}$$

The variation in Eq. (23) with l constitutes a flash energy spectrum.

3. Analysis methodology

a. Calculation of dimensional quantities

For a flash size metric with units of length squared, this study uses the area of the convex hull A_h of the horizontal plan (x, y) projection of VHF source points that belong to the same flash. In 2D, the convex hull is simply the polygon produced by allowing a rubber band to contract on all the points constituting the flash (Devadoss and O'Rourke 2011). The convex hull has the useful property that it is the minimum area that collects all points without requiring assumptions about the degree of permissible concavity, and it allows the flash to define the geometry instead of imposing an assumed form. For flashes that fill space relatively evenly in all directions around the flash centroid, as is most often observed, the chosen metric is quite appropriate and maps well onto an intuitive idea of the area of the storm covered by a flash (Fig. 2).

There is precedent in the literature for the use of the convex hull as a bounding region for objects with geometric character similar to that of lightning flashes. Cuntz et al. (2008) found that the area of the convex hull was useful in distinguishing different types of dendritic nerve cells. Leyvraz (1985) used the convex hull to define limits on the active perimeter for growth of diffusion-limited aggregates. A diffusion-limited aggregation growth model has been applied successfully to lightning flashes (Garik et al. 1987, 1989; Mansell et al. 2002).

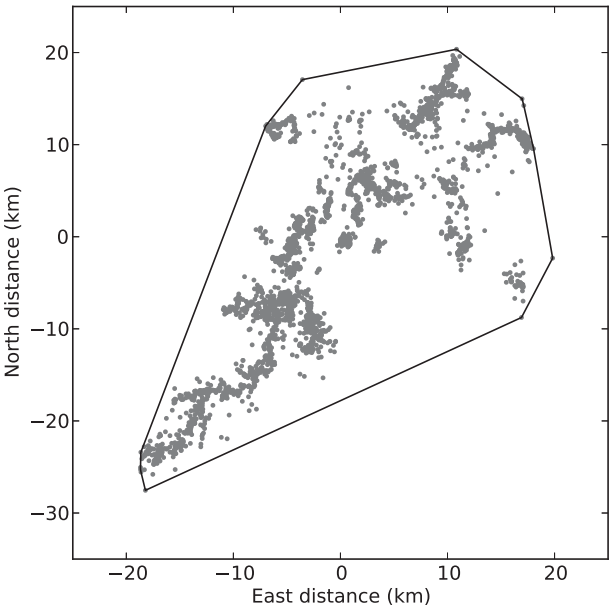

FIG. 2. Example of a flash from 0135:26 UTC 30 May 2004 in plan projection. Distances are relative to the flash centroid. Each gray dot is a VHF source retrieved by the LMA. A solid line connects the subset of VHF sources that define the convex hull. The area of the convex hull in this case is 1038 km^2.

The energy spectrum is calculated using

$$E(l) = \frac{A_h \eta^2}{l_w}. \tag{24}$$

The flash rate at a certain length scale ($l = \sqrt{A_h}$) is calculated by counting flashes in successive size ranges and dividing by the time interval over which those flashes occurred; l_w is the width of the bin used to calculate flash rates. The value of l is taken at the center of the counting bin. To preserve an energetic measure when the spectrum is integrated, the plotted spectrum is divided by l_w for that range of size intervals. (The same spectral shape is obtained when dividing by l instead of l_w.) This approach is analogous to that taken for kinematic energy spectra, which integrates the specific kinetic energy spectrum as a function of wavenumber in units of meters cubed per seconds squared over wavenumber and results in units of meters squared per seconds squared.

b. Flash sorting algorithm

Calculation of flash sizes and rates requires that the VHF source detections be grouped into flashes. The McCaul et al. (2009) flash sorting algorithm is used for this study. The algorithm is similar to many that have been used in recent VHF lightning mapping studies (Wiens et al. 2005; MacGorman et al. 2008). Points are grouped when the distance and time separating pairs of points is less than some threshold value.

The number of flashes counted by the algorithm changes somewhat with the choice of grouping thresholds, especially at large flash rates. Murphy (2006) studied this effect, testing a range of space (1–20 km) and time (0.05–1.00 s) threshold values. They found that flash counts were most stable when thresholds exceeded 5 km and 0.2 s. Flash counts increased rapidly for smaller threshold values. Many studies (Wiens et al. 2005; MacGorman et al. 2008) have used thresholds within the range Murphy (2006) indicated was less stable, but found those counts to compare favorably with counts obtained through painstaking manual, interactive analysis. These past studies have also levied a requirement on minimum number of sources per flash (typically 10) to eliminate those that result from spuriously located sources or real flashes comprising one or a few points. The latter are often observed with surges in supercell updrafts, some of which overshoot the top of the troposphere (Lhermitte and Krehbiel 1979; MacGorman et al. 2008; Bruning et al. 2010; Emersic et al. 2011; Calhoun et al. 2013). These small discharges are not explicitly considered here, since the interpretation of the flash as a flash typically requires some evidence of leader propagation that cannot be resolved with a few points.

To better understand the sensitivity of flash count to algorithm configuration for relatively small separation thresholds, we conducted a test of flash count sensitivity to combinations of 1-, 3-, and 6-km space thresholds and 0.05-, 0.15-, and 0.25-s time thresholds. We also examined the sensitivity of flash counts to minimum source counts of 5, 10, and 20 per flash at constant thresholds of 3 km and 0.15 s.

Tests were conducted on data from 0130 to 0140 UTC 30 May 2004, when the storm in central Oklahoma had extreme flash rates during its mature stage (Calhoun et al. 2013). The results are plotted in Fig. 3, which is dimensionalized in terms of energy instead of count. The general shape of the curves is the same when plotted with units of count, with the dimensional scaling tending to straighten the slope at scales of a few kilometers or less.

For all choices of sorting parameters, the flash energy spectrum shows a peak near or in excess of about 10 km with a rapid decrease in the number of flashes at larger scales. At scales smaller than 10 km, the flash counts decrease more slowly than for large flashes.

For the largest separation parameters, as favored by Murphy (2006), a secondary peak in flash count is produced at flash widths of tens of kilometers. Combinations of shorter separation thresholds do not show this peak. This secondary peak is likely due to spurious grouping of

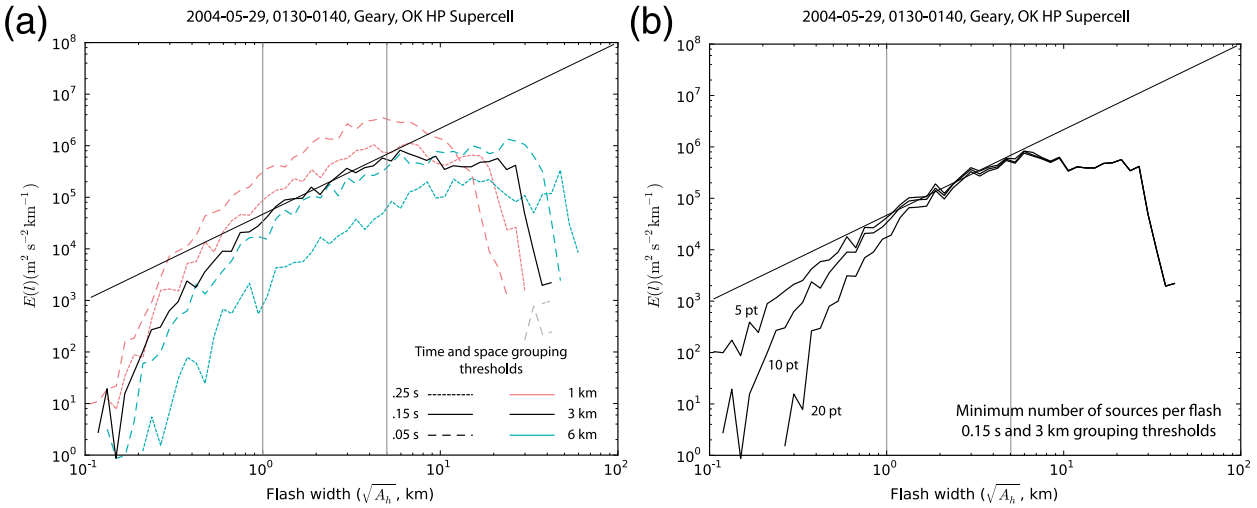

FIG. 3. Flash algorithm sensitivity plots comparing flash counts (dimensionalized in terms of energy) vs the square root of the plan-projection, convex-hull area of each flash. (a) Results for 1-, 3-, and 6-km space thresholds and 0.05-, 0.15-, and 0.25-s time thresholds. Only five of nine possible lines are shown to indicate the envelope of possible curves. (b) Results for minimum source counts of 5, 10, and 20 per flash at constant thresholds of 3 km and 0.15 s. In both (a) and (b) a sloping line represents a $^5/_3$ power-law relationship with the length scale, and vertical lines at 1 and 5 km represent the range of scales where the slope of the spectrum matched the $^5/_3$ line and was relatively insensitive to the flash algorithm's configuration.

smaller flashes, consistent with the shift in flash counts from smaller to larger flashes as flash separation thresholds increase.

For flash sizes less than 1 km and larger than 5 km, the spectral shape changes substantially depending on the choice of minimum number of sources and the space and time grouping thresholds. In between these length scales, the slope of the spectrum is relatively constant.

At small length scales, where the LMA is barely resolving the flashes, the energy spectra fall off more or less rapidly toward zero depending on the threshold chosen for the minimum number of points. The spectrum remains bounded from above by the $-^5/_3$ line determined from larger length scales. The change in the shape of the spectrum is like that produced by different low-pass filter cutoffs, with a larger minimum point requirement resembling a more aggressive filter. Filtering of high-frequency content is common in quality control for other meteorological (kinematic) energy spectra, including those produced from sonic anemometer data and in implicit filtering of the discretized equations in numerical weather prediction models to control the handoff of energy to subgrid parameterizations (e.g., Bryan et al. 2003).

This sensitivity analysis suggests that flash counts between length scales of 1 and 5 km are generally quite stable at this time. Applied algorithms that use lightning flash rate (e.g., Schultz et al. 2009) might find that counts of flashes in or near this size range provide a more stable estimate of trends in the storm-total flash rate. Variations in flash rate would reduce to a single scaling constant represented by a multiplicative coefficient to the power law. The ability to tune the shape of the small-flash-size tail by adjusting grouping thresholds and choosing a minimum number of source points might also prove beneficial.

For the remainder of this study, it may be assumed that the discussion refers to flashes sorted and counted using 3-km spatial and 0.15-s temporal maximum point-to-point separation, with all flashes containing a minimum of 10 points. We make these choices for consistency with past studies, so that the absolute flash numbers are most comparable. The analysis will focus on $l > 1$ km so that the sensitivity to the criteria for minimum number of sources per flash is minimized.

c. *Dataset*

This study uses LMA data from two supercell thunderstorms sampled during the TELEX field campaign (MacGorman et al. 2008). Both storms occurred near the center of the Oklahoma Lightning Mapping Array. The first storm examined was a high-precipitation supercell near Geary, Oklahoma, on the evening of 29 May 2004 (Calhoun et al. 2013). Maximum flash rates were estimated to be roughly 500 min^{-1}. The second storm examined was a classic to low-precipitation supercell (Rasmussen and Straka 1998) that occurred on the evening of 26 May 2004 near Hinton, Oklahoma (Bruning et al. 2010). It was characterized, in its mature stage from 2200 to 0000 UTC, by estimated flash rates of 150 min^{-1}.

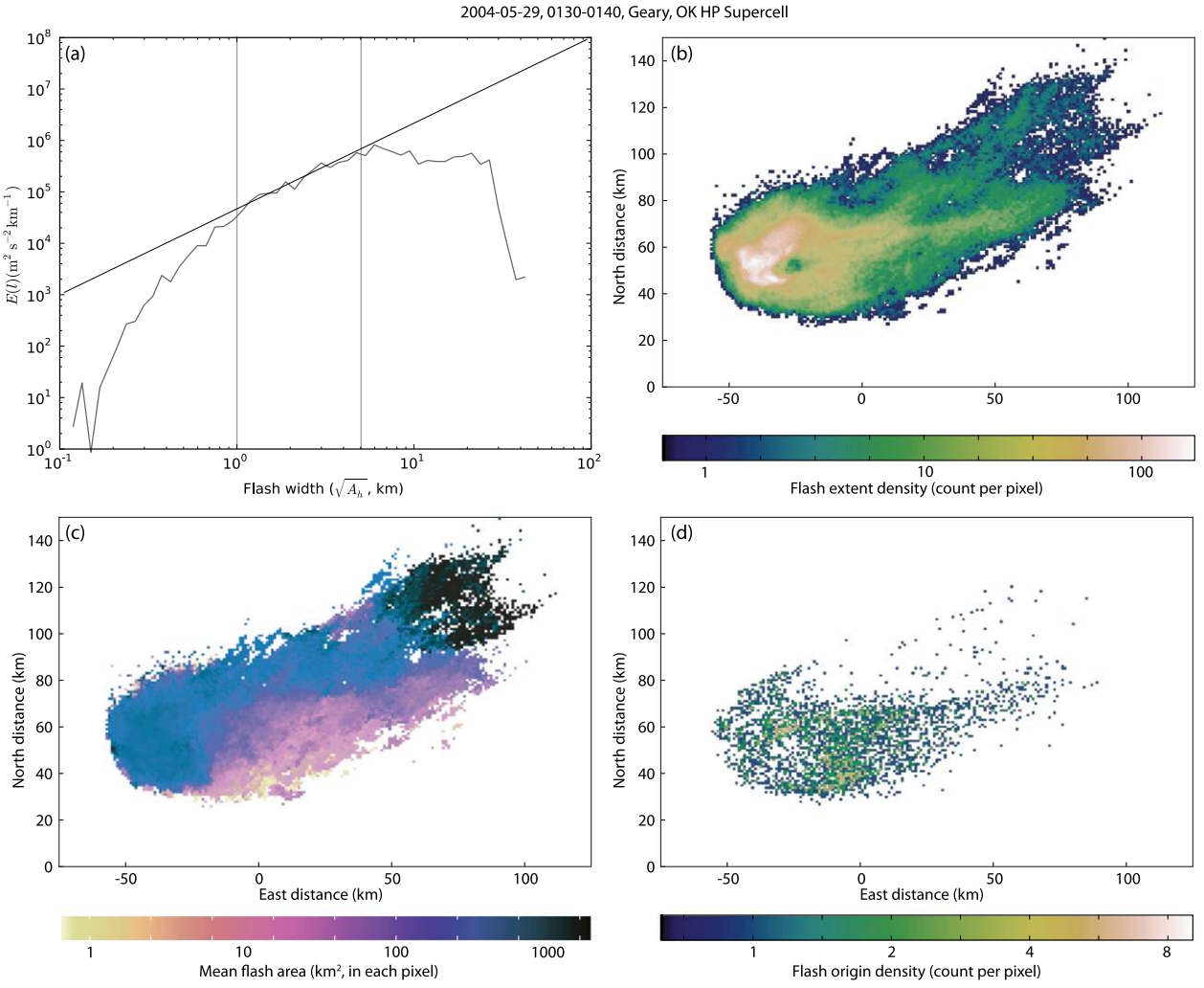

FIG. 4. (a) Whole-storm energetically scaled lightning flash energy spectrum and a line representing a 5/3 power-law relationship with the length scale for 0130–0140 UTC 30 May 2004 in central Oklahoma. This is the 0.15-s, 3-km, 10-point curve from Figs. 3b–d. Plan views of (b) lightning flash extent density, (c) mean flash size per pixel, and (d) flash origin density. Vertical gray lines indicate the region between 1 and 5 km where the rate of change in flash counts is stable across algorithm configurations.

The analysis included 4 h of data centered on the time of each storm's most mature phase. In each 10-min segment during the analysis interval, flashes were sorted and then counted in four ways. An example of each method is shown together for 0130–0140 UTC for the 30 May 2004 supercell (Fig. 4). The dimensionalized flash energy spectrum (Fig. 4a) considers the storm as a whole in order to capture all possible scales of structure caused by the storm's perturbation to its environment. Local flash size and rate variability in their storm-relative context can be seen in Figs. 4b–d. Each panel represents a column-total view of 10 min of lightning data gridded at 1-km resolution. Flash extent density (Fig. 4b) counts the number of flashes passing through a pixel, while the flash footprint plot (Fig. 4c) gives the mean area of the flashes touching that pixel. The flash origin plot (Fig 4d) shows the number of the flashes that began within a pixel. Flash extent and origin density have been previously used by McCaul et al. (2009), while the mean flash area plot is new to this study.

In total, tens of thousands of lightning flashes were analyzed, providing a large database of flashes at different stages in the storms' life cycles and in two of the supercell environments described by Rasmussen and Straka (1998).

4. Results

a. Local flash size distributions

The flash origin and flash footprint grids are useful for testing the claim that the local breakdown rate and

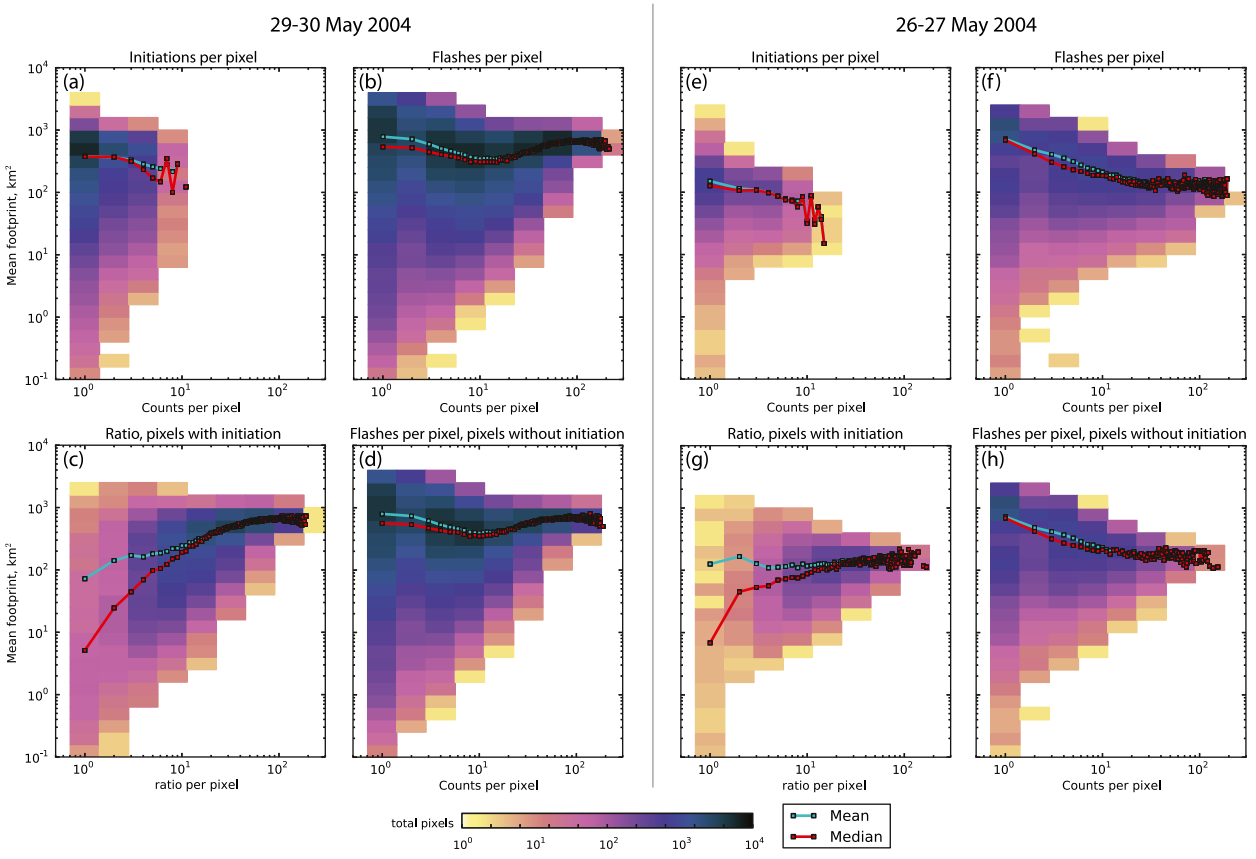

FIG. 5. Distribution of pixels having a given mean flash area (footprint) and flash rate or ratio. The median (red line) and mean (cyan line) of the mean flash footprint at a given flash rate or ratio are plotted at that x-axis value. Data for (a)–(d) 2300–0300 UTC 29–30 May and (e)–(h) 2100–0100 UTC 26–27 May 2004. (a),(e) Flash initiation counts. (b),(f) Flash counts from flash extent density. (c),(g) Ratio of flash counts from flash extent density to the number of flash initiations for those pixels where flashes initiated. (d),(h) Flash counts from flash extent density for those pixels where flash initiations did not occur.

channel extent are opposed. Qualitative evidence for this claim can be seen in the plan-view plots of data from 29 to 30 May 2004 in Figs. 4b–d, where noteworthy features of the data included a lightning hole at coordinates −25 km east, 55 km north and the extensive anvil flashes that propagated downshear 100 km. On the southern flank of the storm, numerous small flashes were situated where a new lightning hole formed over the subsequent hour. In the downshear anvil, north of about 70 km, there were very few flashes, all of which were relatively extensive. To the west and north of the lightning hole, average flash sizes were moderate and relatively uniform; detailed examination of these flashes (not shown) indicated diversity in flash sizes, with high altitudes showing small flashes similar in size to the average to the southeast, while low levels showed extensive flashes. There is also a secondary maximum of singleton sources southwest of the hole at very high altitude, in excess of 15 km.

On the southern flank of the storm in Fig. 4, the region with the greatest number of flash initiations corresponds with the smallest average flash sizes. Only a few flashes are present in the downshear anvil, and flash extents are largest there. These two regions seem to confirm the theoretical inference from basic electrostatics. The region to the north and west of the hole seems to conflict with the electrostatic prediction. However, the averaging of flash areas for all flashes in the column might not have provided the best test in this case, since there was observed systematic variation in the average flash area within the column.

Figure 5 shows aggregate data from each pixel in the 10-min gridded data for both storms. Figures 5a, 5b, 5e, and 5f simply summarize how many pixels (given by the color fill) were found to have certain combinations of mean flash size versus flash initiation (Figs. 5a,e) or flash extent (Figs. 5b,f) density. Note that the mean and median of the mean flash area decreased with increasing flash initiations for both storms, although the curves became noisier for values with the largest number of flash initiations, which had few pixels.

Pixels were further segregated by the presence of any flash initiation. Figures 5d and 5h show mean area versus flash extent density for pixels where no flashes were observed to begin. Statistics for the remaining pixels, where flashes were observed to begin, are plotted in Figs. 5c and 5g, which show counts of pixels having certain combinations of mean area versus the ratio of local flash rate to local flash initiation rate. An initiation-normalized flash rate ratio of 1.0 represents a pixel in which all flash propagations were due to local initiation, while higher ratios represent pixels dominated by propagation through them even if an initiation or two were observed.

The expected average flash area is larger for pixels where flash initiations were a smaller fraction of the total flash count. The effect is especially noticeable in the median curve, as it progresses from pixels with a ratio of 1.0, in which local breakdown dominated the statistics and the median flash area is smaller, to pixels having larger values of the ratio. At larger values of the ratio in both storms, in which propagation through the pixel of flashes that did not initiate there dominated, the median of the average flash areas converges to a moderately high value. Below the median, there is likewise a fairly steady increase in the mean footprint for any given total number of pixels as the ratio increased.

b. *Whole-storm flash size spectra*

Figures 6 and 7 show all of the dimensionalized flash-size spectra for the 26–27 and 29–30 May 2004 supercells during their mature stages. Also plotted is a reference line showing a 5/3 power-law relationship between length scale and specific energy.

1) 29–30 MAY 2004

Figure 6 presents spectra for the entire analysis period on 29–30 May 2004. Representative times are summarized in Fig. 6f and are discussed in detail below.

From 2300 UTC 29 May to 0000 UTC 30 May 2004, the flash energy spectra were relatively similar (Fig. 6a), with a peak at a flash width of about 20 km. Specific energies quickly became smaller at larger flash sizes. The flash energy decrease below 10-km width roughly followed a 5/3 power law until the 1-km flash width cutoff, where the flash sorting algorithm was shown to be susceptible to flash definition choices. At 0000 UTC, flash rates (and therefore energies) were observed to increase substantially across the entire spectrum (Fig. 6b). The peak remained at about 20 km, and the slope of the spectra between 10 and 1 km continued to parallel the 5/3 power-law line.

Another upward trend in flash rate was observed from 0050 to 0150 UTC (Fig. 6c). The spectra were at nearly constant energy from about 7 to 30 km, while the 1–7-km range continued to parallel the 5/3 power-law line. The largest total flash energies of the case were observed in this interval. Between 0150 and 0230 UTC, flash energies decreased once again (Fig. 6d). Spectral shapes were similar to the previous interval, with the exception of a secondary peak at 20–30-km flash width. At 0230 UTC, there was a slight increase in flash energy between 5- and 20-km flash width as the portion of the spectrum that best paralleled the 5/3 line shifted to larger flash sizes (Fig. 6e).

For the 4 h of data analyzed on 29–30 May 2004, a power-law scaling regime in flash energy was observed across a range of flash widths. The scaling regime was typically centered on flash widths of a few kilometers and was present even as flash rates fluctuated.

2) 26–27 MAY 2004

The 29–30 May storm was characterized by large flash rates throughout the entire 4-h analysis period. To better understand the behavior of the spectra at low-to-moderate flash rates, we now examine the storm on 26–27 May 2004. The entire evolution of the 26–27 May storm, from first flashes through decay, was captured in the 4-h analysis interval. Representative times for 26–27 May 2004 are summarized in Fig. 7d and are discussed in detail below.

Prior to 2140 UTC (Fig. 7a), flash rates were low enough that the energy spectra were sparse and noisy. The first spectrum with some structure was produced at 2140–2150 UTC when an average of 19 flashes per minute was present. While the spectrum was less wide and tall in comparison to 29–30 May, there was a resolved peak in the spectrum at 7 km and a possible 5/3 power-law regime from 6–7 km down to 2 km.

From 2140 to 2220 UTC, the trend was toward greater specific energies and a broader range of flash widths (Fig. 7a), as the storm emerged from a dryline-influenced environment and became a chain of strong cells with much larger flash rates of about 100 min^{-1}. The storm began a transition to a supercellular mode at around 2230 UTC (Bruning et al. 2010). The average flash rate from 2220 to 2230 UTC was 103 min^{-1}, with a spectral peak at 10 km and a 5/3 scaling regime from about 1 to 10 km. The spectral shape fluctuated from 2220 to 2320 UTC (Fig. 7b), with $E(l)$ at the scale of a few kilometers varying between the value at 2140 UTC and the value at 2220 UTC. A spectral peak was maintained at about 10-km flash width.

The spectral peak and power-law scaling regime moved to smaller flash widths from 2320 to 0010 UTC (Fig. 7c). The peak was at 3 km by 0000–0010 UTC. At 0010–0020 UTC, with flash rates averaging 26 min^{-1}, the spectral peak was between 1 and 2 km, with $E(l)$ diminishing slowly from 10^3 to 10^2 $\text{J kg}^{-1}\,\text{km}^{-1}$ for flash

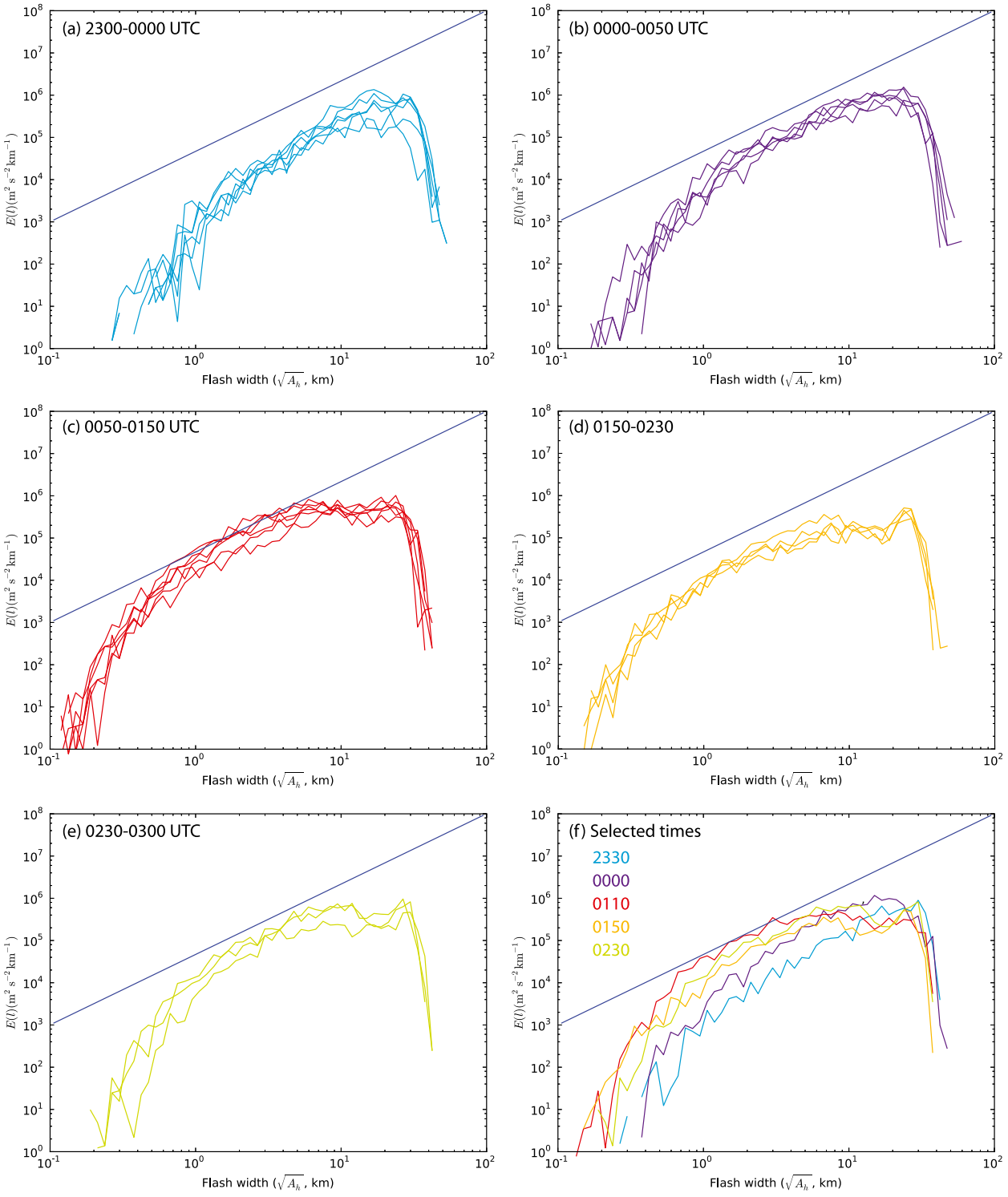

FIG. 6. Whole-storm energetically scaled lightning flash size spectra and a line representing a $^5/_3$ power-law relationship with the length scale for 29–30 May 2004 in central Oklahoma. Each spectrum represents 10 min of data, covering (a) 2300–0000, (b) 0000–0050, (c) 0050–0150, (d) 0150–0230, and (e) 0230–0300 UTC. (f) Selected times: 2330 (blue), 0000 (purple), 0110 (red), 0150 (orange), and 0230 UTC (green).

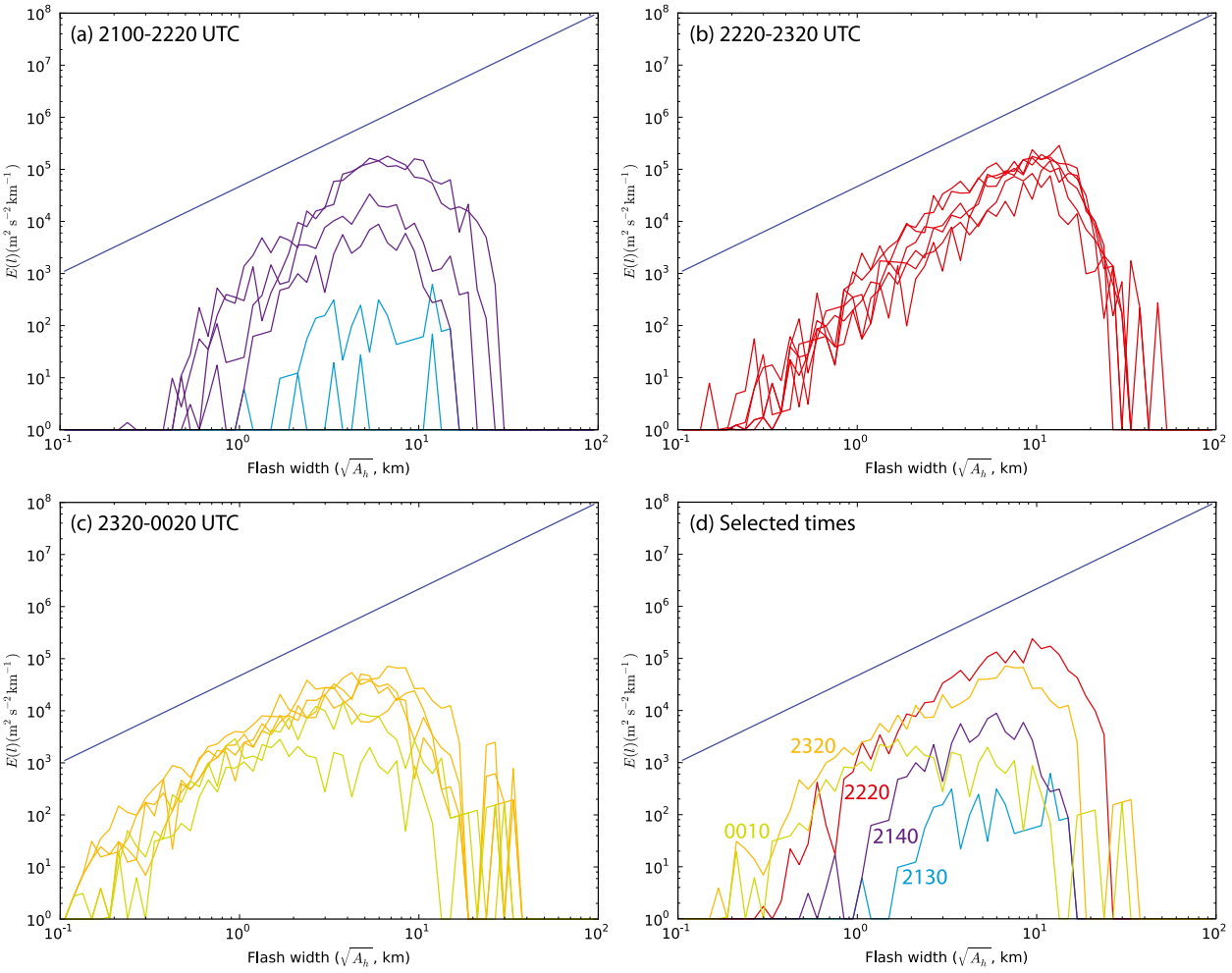

FIG. 7. Whole-storm energetically scaled lightning flash size spectra and a line representing a 5/3 power-law relationship with the length scale for 26–27 May 2004 in central Oklahoma. Each spectrum represents 10 min of data, covering (a) 2100–2140 (light blue) and 2140–2220 (purple), (b) 2220–2320, and (c) 2320–0000 (orange) and 0000–0020 (green) UTC. (d) Selected times: 2130 (blue), 2140 (purple), 2220 (red), 2320 (orange), and 0010 (green) UTC.

widths above 2 km and below 10 km. After 0020 UTC, the average flash rate dropped to less than 10 $\mathrm{min^{-1}}$, and the spectrum became too undersampled to interpret as the storm continued to decay toward 0100 UTC. Only two flashes occurred in the interval 0050–0100 UTC and had widths of about 10 km.

The behavior of the spectra at lower flash rates in the 26 May storm rates raises questions about whether a consistent spectral shape simply requires a large-enough sample of flashes, or whether the electrical and convective dynamics themselves change at some flash-rate threshold.

5. Discussion

The examination of local flash statistics (Fig. 5) for both storms appears to confirm the prediction that average local flash area and local breakdown rate are opposed. The data support an expectation that pixels with a high (low) flash initiation rate would have smaller (larger) average flash sizes. An extension of the methodology in this study to three-dimensional pixels would control for systematic variability with height in flash size in the columns northwest of the lightning hole. The fact that there is a detectable difference even with column-average conditions suggests a difference substantial enough to overcome the blurring of vertical structure inherent in our analysis methodology.

The energetically scaled flash size spectra were found to have two noteworthy characteristics. First, the spectra had peaks at l on the order of 10 km. Those spectral peaks were found at scales on the order of the cell size for the two storms studied and were larger for the larger storm on 29 May. Second, it was typical to find a power-law

scaling regime, below the spectral peak, with a slope close to $^5/_3$. The range of scales spanned by this power-law regime fluctuated, especially for the 26 May storm. The energy spectrum was observed to fall off much more rapidly at larger scales than at smaller ones. As flash rates increased, the spectral height tended to rise, and vice versa, which is not surprising given that the definition of $E(l)$ included flash rate.

The maintenance of the basic spectral shape as the storm's intensity fluctuated is noteworthy, and for the rest of this study we will concern ourselves with some speculation about why a power-law scaling regime and spectral peak might be found at the observed scales. Having laid out the general contours of the argument here, future studies might wish to further investigate detailed causal links between flash size spectra fluctuations and thunderstorm dynamics.

a. Convective organization of electric potential

Earlier, we posed the question of the extent to which the electrical and kinematic systems are coupled in thunderstorms. Of particular interest are the motions of the charge-carrying hydrometeors embedded in the thunderstorm's flow.

Gravitation is responsible for the initial downward acceleration of precipitating hydrometeors but acts only over a short distance (length scales on the order of 1 m; Wang and Pruppacher 1977) before gravitation is balanced by air drag, and does not always act opposite the electric field. Furthermore, Doppler radar studies of precipitation fall speeds before and after lightning flashes, where the electrical force suddenly changes, in combination with calculations of available gravitational potential suggest that the gravitational contribution is generally too small to explain portions of the storm observed to be significantly electrified (Williams and Lhermitte 1983; Williams 1985; Weinheimer 1987).

Thunderstorm convection is driven by the release of latent heat, thereby realizing buoyant potential instability, creating an upward-moving region of air that perturbs its environment (referred to as the convective plume). A horizontal gradient in vertical motion also generates shear stresses along the interface between the convective plume and the wider environment, producing a cascade of turbulent eddies. Such eddies can be responsible for producing differential accelerations between precipitating and nonprecipitating hydrometeors, as in the following illustration. Imagine a group of precipitating, electrified hydrometers that are detrained from the gross convective plume. The plume itself still contains oppositely electrified, nonprecipitating hydrometeors, which accelerate away from the precipitating hydrometeors as long as buoyant forcing continues. In the fully turbulent convective plume, a range of eddy sizes exist, with abundant opportunities for transfer of hydrometeors from eddy to eddy and for associated relative acceleration. Based on this reasoning, we would expect a storm's electrical energy to derive, ultimately, from the convective motions, and that the convective motions might serve to organize the potential distribution discharged by flashes. Such an expectation is intuitively satisfying. The release of thermal conditional instability in the form of convective motions is the very reason why a storm exists at all, so it is reasonable to expect the electrical energy to derive from the energy contained in convection.

The expected link between convective energy and electrical energy has motivated numerous searches for relationships between lightning activity and bulk thunderstorm quantities like storm height, updraft mass flux, maximum updraft speed, etc. (e.g., Boccippio 2002; Wiens et al. 2005; Kuhlman et al. 2006; Tessendorf et al. 2007; Barthe et al. 2010; Deierling et al. 2008; Deierling and Petersen 2008; Dolan and Rutledge 2010). The theme of how lightning couples to the convective plume is extended and synthesized here by considering eddy-scale aspects of the plume structure.

b. Electric potential structure and flash characteristics

The discussion accompanying Fig. 1 mentioned the importance of understanding the production of structure in the potential field since it is closely linked to the local electrical breakdown rate and the extent of the flashes that develop.

One method of producing a high-complexity potential distribution is through turbulent stretching and folding of parcels of air within the thunderstorm. One might imagine a moderately large turbulent eddy carrying negative charge that moves upward through a region of uniform positive charge. As it moves upward, a tendril of this eddy curls over, and in the horizontal cross section perforates the positive charge with a pocket of negative charge.

In a real (nonidealized) thunderstorm, there is a continuum of eddy sizes. One way of understanding the character of the turbulent eddies in thunderstorms is with the turbulent kinetic energy (TKE) spectrum for vertical velocity, as done in Bryan et al. (2003). In those simulations in which the TKE spectrum was reasonably well resolved according to large-eddy simulation principles, conserved scalar fields such as equivalent potential temperature showed considerable eddy structure, while less-resolved simulations showed highly smoothed fields. In much the same way, the same turbulent kinematics could be expected to redistribute electrical potential (another scalar field), which is coupled to the charge carried on hydrometeors present in the storm flow.

Kinetic energy spectra in fluids with large Reynolds number are expected to follow a $-5/3$-wavenumber power law in an inertial subrange at less than some critical wavelength (Kolmogorov 1941). Above this range (e.g., thunderstorm anvil outflows), there is a handoff of energy from three-dimensional turbulence to stratified, two-dimensional, possibly turbulent flow (Lilly 1983). The subrange at large wavenumbers characterizes a downscale cascade of energy from larger to smaller eddies. In the thunderstorms simulated by Bryan et al. (2003) the TKE peak was at about 10 km, with an inertial subrange modeled between 1 and 10 km. The model's inherent dissipative filter scale prevented assessment of the spectrum at scales smaller than about 1 km. They noted that there is still considerable uncertainty in where the inertial subrange truly begins in deep convection.

The LMA-derived flash energy spectra look remarkably similar to a thunderstorm's TKE spectrum, including the $5/3$ slope where the inertial subrange is expected to begin, and a peak at approximately 10 km.

There are several possible explanations for the similarity between kinematic and electrical energy spectra in thunderstorms. The foremost question that merits further investigation is whether the turbulent kinematics really control the texture of the charge distribution inside storms, thereby impacting the flash size and rate distribution. Past studies have found links between net charge structure, lightning propagation, and storm-relative charge advection (section 1), and this study suggests the need to investigate whether charge advection effects continue to dominate at the most granular length scales considered here. Perhaps it is also possible that the same mathematics of energy conservation apply to both the electrical and kinematic forms and necessarily produce the same energy spectrum at the same scales, without necessarily requiring that the kinematic energetics influence and organize the electrical energetics.

The charge budget at any point in the storm depends on several factors in addition to advection of charge. The largest include microphysical charge separation (especially between graupel and ice crystals in the presence of supercooled water; Takahashi 1978; Saunders et al. 2006), charge sedimentation (due to differential fall speeds of hydrometeors), and the charge deposited by lightning itself (which is usually of the opposite sign of the charged region through which the channel moves). For sufficiently large charging rates (which would be accompanied by the large flash rates at which the spectra were found to be most consistent), the required discharge rate may be so large that flashes become nearly simultaneous and space filling across the entire storm core, as observed in supercells. Such behavior might constitute an electrical analog to the turbulent breakdown of flow at high Reynolds number, where the electrical stress acts analogously to the fluid stresses that give way at the onset of turbulence.

If the electrical and kinematic characteristics are not closely coupled and a comparable scaling subrange is found in the electrical data, then a purely electrodynamic explanation would be necessary to explain the electrostatic spatial structure.

Is it possible to explain these observations using a purely electrical mechanism, divorced from the storm flow? Consider the following thought experiment that begins with a uniform charge distribution in two uniform layers. At some point, a flash forms and propagates tortuously through each uniform charge layer. This flash propagation deposits some new charge within the two initial layers, which we expect, by the branched nature of the lightning channel, to create a more pocketed potential field. Assume now that this new potential field is amplified uniformly by some mechanism until the next flash or flashes take place. These flashes continue to fill the pockets not discharged by the first flash. This produces the desired cascade of flash sizes, on down to the scale where ionic transport accomplishes the final dissipation of electrical energy.

However, the above argument elides some important facts about the charging and discharge process. To raise the electric field back up to breakdown strength for more flashes, charge must be separated through a precipitation-based mechanism. These hydrometeors are embedded in the flow of the storm. Furthermore, the tortuous flash propagation itself exhibits a dendritic structure characterized by a diffusion-limited aggregation process. The gaseous constituents of the atmospheric fluid are what act to limit ion diffusion.

Therefore, even in attempting to describe a purely electrical energy cascade, we are forced to return to the role of the atmospheric fluid in sustaining the flash rate and controlling the tortuous geometry of flashes. It is therefore reasonable to expect to find evidence for strong coupling between the electrical and fluid constituents of a thunderstorm. That this fluid is constantly in motion cannot be ignored.

c. *Further justification of the dimensional flash energy combination*

It is possible to incorporate the coupling between the convective generator of electrical energy into the capacitor model of a lightning flash. By doing so, further justification is provided for the choice of dimensional combination in Eq. (23).

For a capacitor with capacitance

$$C = \frac{\epsilon_0 A}{d}, \tag{25}$$

the total energy W dissipated for charge Q is

$$W = \frac{Q^2}{2C}. \tag{26}$$

For an average charging current I between successive individual flashes at an interval of T seconds, $Q = IT$ and

$$W = \frac{I^2 d}{2\epsilon_0 A} T^2. \tag{27}$$

For a capacitor, where the charging current is delivered to area A, one may define $I = JA$, so

$$W = \frac{J^2 A d}{2\epsilon_0} T^2. \tag{28}$$

Assume that the charging current is provided by some convective velocity $w = d/T$ acting on a charge gradient in the z direction (where z defined in the direction of d), and

$$J = \frac{I}{A} = \frac{w}{A}\frac{\partial Q}{\partial z}, \tag{29}$$

which is a charge flux that may also be written as

$$J = w\rho = \frac{\rho d}{T}. \tag{30}$$

Therefore,

$$W = \frac{\rho^2 A d^3}{2\epsilon_0}. \tag{31}$$

For some constant background net charge density, the charge flux can be thought of as the capture of the background charge density on the capacitor's plates as they separate in the flow through the background charge density. The total charge is the charge density times the volume formed by the separation of the plates.

To consider an ensemble of flashes, divide the total volume V_I formed by the plate separation into subvolumes V_i. Each individually discharging region subdivides the total area A_I into identical flash areas A_i. Then, each flash is responsible for a fraction Q_i of the total charge,

$$Q_i = \rho V_i. \tag{32}$$

The total volume is

$$V_I = V_i \eta_i T, \tag{33}$$

which gives

$$\rho = \frac{Q_i \eta_i T}{V_I}. \tag{34}$$

Therefore, the total energy dissipated at size scale A_i is

$$W_i = \frac{1}{2}\frac{Q_i^2}{\epsilon_0}\frac{A_i d^3}{V_I^2}\eta_i^2 T^2. \tag{35}$$

To normalize the flash energy per unit mass of air, note that $m = \rho_a V_I$, where ρ_a is the density of air, giving

$$E_W = \frac{W_i}{\rho_a V_I} = \frac{1}{2}\frac{Q_i^2}{\rho_a \epsilon_0}\frac{d^3}{V_I^3} A_i \eta_i^2 T^2. \tag{36}$$

Equation (36) is proportional to A_i and η^2, as suggested by dimensional analysis, and arose from a simple model that is a good approximation observed flash morphology. The derivation also explicitly couples the storm's convective motions to charging current through a highly simplified model of charge advection.

It would be valuable for a future study to examine the influence of Q_i and d on E_W. The LMA does not measure Q_i, though it could be estimated from electric field change (Lu et al. 2011) or direct charge moment change (Cummer and Lyons 2004; Lu et al. 2012) observations. Estimates of d are possible from the LMA, but errors in source altitudes increase much faster with range than the plan position errors. Sloped charge layers also complicate estimates of flash depth. These sources of error in d are easily of the same order of magnitude as d itself, and therefore a much less robust estimate than A. Finally, the physical variation in d (of order 1 km) is much less than that in A (ranging from 1 to 100 km), suggesting that it is reasonable to treat d as a constant.

d. Storm-relative flash properties

In Fig. 4 the patterns in the lightning data matched well with expected eddy characteristics inferred from the observed kinematics in the 29 May 2004 storm. The general patterns in the lightning data were observed to hold throughout the 4 h analyzed. Calhoun et al. (2013) reported, in a detailed case study of the earlier 0000–0100 UTC interval, that concentrated vertical velocity maxima remained mostly along and south of the lightning hole through midlevels, while at upper levels the lightning activity was centered on the updraft maximum. The deep, intense updraft on the storm's right flank would be expected to contain the most turbulence,

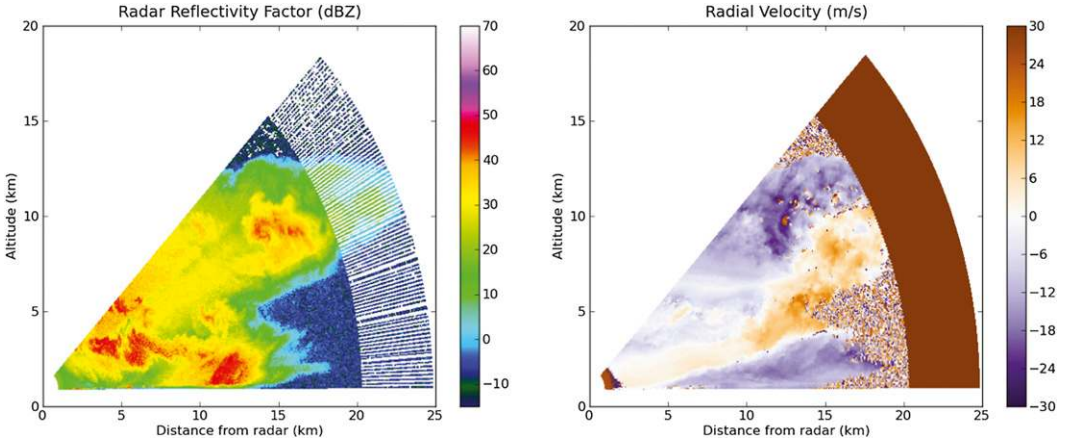

FIG. 8. Radar reflectivity factor and unedited radial velocity data in a vertical (range–height indicator) section through a squall line at 0020:55 UTC 22 Oct 2010 near Lubbock, Texas. Note that the radar signal completely attenuates between 15 and 20 km in the lower half of the image, where radar reflectivity factor drops below 0 dBZ and the velocity field becomes incoherent. Inflow rises over a cold pool advancing toward the radar and turns upward into a deep convective plume with an overturning rotor and embedded smaller-scale turbulence at 15-km range, while relatively smooth, stratified flow can be seen at 6–7-km altitude between 5- and 10-km range.

while the increasingly stratified kinematic structure toward the forward anvil exhibited the most extensive flashes. The vertical variation in flash structure observed northwest of the lightning hole was also qualitatively consistent with the observed storm kinematics. Immediately northwest of the lightning hole, vertical velocities at 6 km rapidly decreased to a nearly uniform $\pm 3\,\mathrm{m\,s^{-1}}$, while aloft updraft was present. A turbulent upper-level updraft (into the overshooting top) would be consistent with a highly structured potential field and small flashes; at the same time, sedimenting, detraining precipitation near the surface to the north and west could have organized potential into larger structures.

In contrast with the persistently high flash rates in the 29 May supercell, it is worth remarking on the expected lightning energy spectra in low-flash-rate storms. The same TKE spectral shapes would be expected in any convective plume, including low-flash-rate thunderstorms, but the spectra on 26 May 2004 (Fig. 7) showed that the flash-derived electrical energy spectra are poorly resolved at low flash rates. However, Bruning et al. (2007) provide some clues that our general reasoning about the organization of electrical potential by the convective eddy texture still applies. Bruning et al. (2007) used LMA and polarimetric radar data to study a thunderstorm that grew and decayed in a weak multicellular mode. That storm's flash rate was about $1\,\mathrm{min^{-1}}$, comparable to the early and late stages of the storm on 26–27 May 2004. They noted that flashes during an active convective pulse were relatively compact and remained separated within each cell in a small ensemble of cellular features in reflectivity. Later, as convective activity subsided, individual flashes extended across the ensemble of cells. They also noted that the LMA sources were more diffuse in appearance as convection subsided, while earlier flashes were tortuous on about the same scale as localized maxima and minima in the polarimetric fields.

A future study of storms having the lower flash rates typical of multicellular convection would control for the any influence of (extreme) charging and discharge rates on charge granularity and help isolate the role of convective eddy structure. If a similar spectral shape were resolved over longer averaging durations for a single cell or over a larger spatial domain for an ensemble of cells, it would help rule out a per-storm-cell flash rate threshold below which the $-5/3$ spectra does not apply. Furthermore, LMA-derived evidence that texture exists is contingent on the presence of flashes. The fact that flash initiation only takes place above a certain local electrical potential energy difference threshold should also be accounted for in future work.

We suggest that the fields in Figs. 4b–d may be considered to be a set of ''base data'' for total lightning measurements, in that they seek to represent aspects of the distribution, organization, and evolution of the basic electrostatic quantities in thunderstorms. While constructed in 2D in this case, 3D fields might allow additional refinement to whole-storm and storm-relative flash size relationships. In operational settings, product users who seek to assimilate lightning data into their mental model of internal storm dynamics may find such views of lightning data helpful, inasmuch as they enable at-a-glance correlations to storm structure and kinematic reasoning about charge transport.

6. Concluding remarks

This study shows that a 5/3 power law exists in an energetically scaled lightning flash energy spectrum on a length scale of a few kilometers. The spectral peak was near 10 km. These spectral characteristics appear to be a persistent feature of supercell thunderstorms with moderate-to-large flash rates. The spectral shapes and local flash statistics for 8 h of data from two different supercell storms were similar and surprisingly consistent. One of the storms was weaker and underwent significant growth and decay during the analysis period, providing insight about the flash rates necessary to produce the well-resolved electrical energy spectra seen in more robust convection.

The sizes spanned by the scaling regime and the peak in the energy distribution are comparable to those expected for the kinetic energy inertial subrange in thunderstorms. The correspondence between kinematic and electrical properties suggests that advection of charge-bearing precipitation by the storm's flow couples the electrical and kinematic properties of a thunderstorm.

The data also support a possible correspondence between the eddy-controlled texture of electrical parameters and flash properties. Column-total statistics verify an electrostatic prediction that regions dominated by frequent lightning initiation correspond to small flashes, and vice versa. Plan views of flash size distributions in a storm-relative sense also suggest practical applications for assessing the local convective character through modulations in flash size and rate.

This study also suggests the need for an observing campaign focused on the kinematic texture of thunderstorms, which would enable a direct comparison of the kinematic and electrical characteristics in different storm-relative locations at a range of scales. Variability in the electric field and winds along paths through storms penetrated with aircraft or balloons would be one route to evaluating these hypotheses, although the sparse temporal and spatial sampling of these methods presents challenges. Another possible method might be to analyze high-resolution, rapidly updating vertical scans with a Doppler weather radar within the coverage of a Lightning Mapping Array. Some preliminary observations with the Texas Tech University mobile Ka-band radars clearly resolve highly turbulent flow in and near deep convective updrafts and relatively smooth-appearing flow regimes farther away from the overturning of the deep convective plume (Fig. 8). Although these radars attenuate strongly, the small beamwidth gives obvious sensitivity to the turbulent character on small scales as well as the large-eddy rotor at 15-km range and 10-km altitude. While from a different case than that studied here, Fig. 8 provides a helpful illustration of the convective character that might control charge transport on both fine and large scales.

Acknowledgments. This work was supported by COMET and the GOES-R program under Award Z11-91820 and by the National Science Foundation under Grants 0924621 and 1063966. Bill McCaul provided the flash algorithm code. We also thank Ted Mansell, Kristin Calhoun, Paul Krehbiel, Song-Lak Kang, and Christopher Weiss for fruitful discussions that helped refine ideas in this study. We acknowledge the comments provided by several anonymous reviewers, whose suggestions helped improve the manuscript. Thanks to John Schroeder and Scott Gunter for providing the TTUKa data.

REFERENCES

Barthe, C., W. Deierling, and M. C. Barth, 2010: Estimation of total lightning from various storm parameters: A cloud-resolving model study. *J. Geophys. Res.,* **115,** D24202, doi:10.1029/2010JD014405.

Boccippio, D. J., 2002: Lightning scaling relations revisited. *J. Atmos. Sci.,* **59,** 1086–1104.

Braham, R. R., Jr., 1952: The water and energy budgets of the thunderstorm and their relation to thunderstorm development. *J. Meteor.,* **9,** 227–242.

——, 1953: The energy of thunderstorm electrical activity. *Pure Appl. Geophys.,* **25,** 221–222, doi:10.1007/BF02014068.

Bruning, E. C., W. D. Rust, T. J. Schuur, D. R. MacGorman, P. R. Krehbiel, and W. Rison, 2007: Electrical and polarimetric radar observations of a multicell storm in TELEX. *Mon. Wea. Rev.,* **135,** 2525–2544.

——, ——, D. R. MacGorman, M. I. Biggerstaff, and T. J. Schuur, 2010: Formation of charge structures in a supercell. *Mon. Wea. Rev.,* **138,** 3740–3761.

Bryan, G. H., J. C. Wyngaard, and J. M. Fritsch, 2003: Resolution requirements for the simulation of deep moist convection. *Mon. Wea. Rev.,* **131,** 2394–2416.

Calhoun, K. M., D. R. MacGorman, C. L. Ziegler, and M. I. Biggerstaff, 2013: Evolution of lightning activity and storm charge relative to dual-Doppler analysis of a high-precipitation supercell storm. *Mon. Wea. Rev.,* **141,** 2199–2223.

Carey, L. D., M. J. Murphy, T. L. McCormick, and N. W. Demetriades, 2005: Lightning location relative to storm structure in a leading-line trailing stratiform mesoscale convective system. *J. Geophys. Res.,* **110,** D03105, doi:10.1029/2003JD004371.

Coleman, L. M., T. C. Marshall, M. Stolzenburg, T. Hamlin, P. R. Krehbiel, W. Rison, and R. J. Thomas, 2003: Effects of charge and electrostatic potential on lightning propagation. *J. Geophys. Res.,* **108,** 4298, doi:10.1029/2002JD002718.

Cummer, S. A., and W. A. Lyons, 2004: Lightning charge moment changes in U.S. High Plains thunderstorms. *Geophys. Res. Lett.,* **31,** L05114, doi:10.1029/2003GL019043.

Cuntz, H., F. Forstner, J. Haag, and A. Borst, 2008: The morphological identity of insect dendrites. *PLoS Comput. Biol.,* **4,** e1000251, doi:10.1371/journal.pcbi.1000251.

Deierling, W., and W. A. Petersen, 2008: Total lightning activity as an indicator of updraft characteristics. *J. Geophys. Res.,* **113,** D16210, doi:10.1029/2007JD009598.

——, ——, J. Latham, S. Ellis, and H. J. Christian, 2008: The relationship between lightning activity and ice fluxes in thunderstorms. *J. Geophys. Res.,* **113,** D15210, doi:10.1029/2007JD009700.

Devadoss, S. L., and J. O'Rourke, 2011: *Discrete and Computational Geometry.* Princeton University Press, 280 pp.

Dolan, B., and S. A. Rutledge, 2010: Using CASA IP1 to diagnose kinematic and microphysical interactions in a convective storm. *Mon. Wea. Rev.,* **138,** 1613–1634.

Ely, B. L., R. E. Orville, L. D. Carey, and C. L. Hodapp, 2008: Evolution of the total lightning structure in a leading-line, trailing-stratiform mesoscale convective system over Houston, Texas. *J. Geophys. Res.,* **113,** D08114, doi:10.1029/2007JD008445.

Emersic, C., P. L. Heinselman, D. R. MacGorman, and E. C. Bruning, 2011: Lightning activity in a hail-producing storm observed with phased-array radar. *Mon. Wea. Rev.,* **139,** 1809–1825.

Garik, P., K. Mullen, and R. Richter, 1987: Models of controlled aggregation. *Phys. Rev.,* **35A,** 3046–3055, doi:10.1103/PhysRevA.35.3046.

——, D. Barkey, E. Ben-Jacob, E. Bochner, N. Broxholm, B. Miller, B. Orr, and R. Zamir, 1989: Laplace- and diffusion-field-controlled growth in electrochemical deposition. *Phys. Rev. Lett.,* **62,** 2703–2706, doi:10.1103/PhysRevLett.62.2703.

Kasemir, H. W., 1960: A contribution to the electrostatic theory of a lightning discharge. *J. Geophys. Res.,* **65,** 1873–1878.

Kolmogorov, A. N., 1941: The local structure of turbulence in incompressible viscous fluid for very large Reynolds numbers. *Dokl. Akad. Nauk SSSR,* **30,** 301–305.

Krehbiel, P. R., R. J. Thomas, W. Rison, T. Hamlin, J. Harlin, and M. Davis, 2000: GPS-based mapping system reveals lightning inside storms. *Eos, Trans. Amer. Geophys. Union,* **81,** 21–25.

Kuhlman, K. M., C. L. Ziegler, E. R. Mansell, D. R. MacGorman, and J. M. Straka, 2006: Numerically simulated electrification and lightning of the 29 June 2000 STEPS supercell storm. *Mon. Wea. Rev.,* **134,** 2734–2757.

——, D. R. MacGorman, M. I. Biggerstaff, and P. R. Krehbiel, 2009: Lightning initiation in the anvils of two supercell storms. *Geophys. Res. Lett.,* **36,** L07802, doi:10.1029/2008GL036650.

Lang, T. J., and Coauthors, 2004: The Severe Thunderstorm Electrification and Precipitation Study. *Bull. Amer. Meteor. Soc.,* **85,** 1107–1125.

Leyvraz, F., 1985: The 'active perimeter' in cluster growth models: A rigorous bound. *J. Phys.,* **18A,** L941, doi:10.1088/0305-4470/18/15/007.

Lhermitte, R., and P. R. Krehbiel, 1979: Doppler radar and radio observations of thunderstorms. *IEEE Trans. Geosci. Electron.,* **17,** 162–171.

Lilly, D. K., 1983: Stratified turbulence and the mesoscale variability of the atmosphere. *J. Atmos. Sci.,* **40,** 749–761.

Lu, G., W. P. Winn, and R. G. Sonnenfeld, 2011: Charge transfer during intracloud lightning from a time-dependent multidipole model. *J. Geophys. Res.,* **116,** D03209, doi:10.1029/2010JD014495.

——, S. A. Cummer, R. J. Blakeslee, S. A. Weiss, and W. H. Beasley, 2012: Lightning morphology and impulse charge moment change of high peak current negative strokes. *J. Geophys. Res.,* **117,** D04213, doi:10.1029/2011JD016890.

Lund, N. R., D. R. MacGorman, T. J. Schuur, M. I. Biggerstaff, and W. D. Rust, 2009: Relationships between lightning location and polarimetric radar signatures in a small mesoscale convective system. *Mon. Wea. Rev.,* **137,** 4151–4170.

MacGorman, D. R., and Coauthors, 2008: TELEX: The Thunderstorm Electrification and Lightning Experiment. *Bull. Amer. Meteor. Soc.,* **89,** 997–1013.

——, A. A. Few, and T. L. Teer, 1981: Layered lightning activity. *J. Geophys. Res.,* **86** (C10), 9900–9910.

——, J. M. Straka, and C. L. Ziegler, 2001: A lightning parameterization for numerical cloud models. *J. Appl. Meteor.,* **40,** 459–478.

——, W. D. Rust, P. R. Krehbiel, W. Rison, E. C. Bruning, and K. Wiens, 2005: The electrical structure of two supercell storms during STEPS. *Mon. Wea. Rev.,* **133,** 2583–2607.

Maggio, C. R., and Coauthors, 2005: Lightning-initiation locations as a remote sensing tool of large thunderstorm electric field vectors. *J. Atmos. Oceanic Technol.,* **22,** 1059–1068.

Mansell, E. R., D. R. MacGorman, C. L. Ziegler, and J. M. Straka, 2002: Simulated three-dimensional branched lightning in a numerical thunderstorm model. *J. Geophys. Res.,* **107** (D9), doi:10.1029/2000JD000244.

Marshall, T. C., M. Stolzenburg, C. R. Maggio, L. M. Coleman, P. R. Krehbiel, T. Hamlin, R. J. Thomas, and W. Rison, 2005: Electric field magnitudes and lightning initiation in thunderstorms. *J. Geophys. Res.,* **100** (D4), 7097–7103.

Mazur, V., 2002: Physical processes during development of lightning flashes. *C. R. Phys.,* **3,** 1393–1409.

——, and L. H. Ruhnke, 1993: Common physical processes in natural and artificially triggered lightning. *J. Geophys. Res.,* **94** (D7), 12 913–12 930.

McCaul, E. W., S. J. Goodman, K. M. LaCasse, and D. J. Cecil, 2009: Forecasting lightning threat using cloud-resolving model simulations. *Wea. Forecasting,* **24,** 709–729.

Mo, Q., J. H. Helsdon, and W. P. Winn, 2002: Aircraft observations of the creation of lower positive charges in thunderstorms. *J. Geophys. Res.,* **107** (D22), 4616–4630.

Murphy, M., 2006: When flash algorithms go bad. Preprints, *First Int. Lightning Meteorology Conf.,* Tucson, AZ, Vaisala. [Available online at http://www.vaisala.com/en/events/ildcilmc/Documents/When%20Flash%20Algorithms%20Go%20Bad.pdf.]

Rasmussen, E. N., and J. M. Straka, 1998: Variations in supercell morphology. Part I: Observations of the role of upper-level storm-relative flow. *Mon. Wea. Rev.,* **126,** 2406–2421.

Ray, P. S., D. R. MacGorman, W. D. Rust, W. L. Taylor, and L. Walters-Rasmussen, 1987: Lightning location relative to storm structure in a supercell storm and a multicell storm. *J. Geophys. Res.,* **92** (D5), 5713–5724.

Rust, W. D., W. L. Taylor, and D. MacGorman, 1982: Preliminary study of lightning location relative to storm structure. *AIAA J.,* **20,** 404–409, doi:10.2514/3.51084.

——, and Coauthors, 2005: Inverted-polarity electrical structures in thunderstorms in the Severe Thunderstorm Electrification and Precipitation Study. *Atmos. Res.,* **76,** 247–271.

Saunders, C. P. R., H. Bax-Norman, C. Emersic, E. E. Avila, and N. E. Castellano, 2006: Laboratory studies of the effect of cloud conditions on graupel/crystal charge transfer in thunderstorm electrification. *Quart. J. Roy. Meteor. Soc.,* **132,** 2653–2673.

Schultz, C. J., W. A. Petersen, and L. D. Carey, 2009: Preliminary development and evaluation of lightning jump algorithms for the real-time detection of severe weather. *J. Appl. Meteor. Climatol.,* **48,** 2543–2563.

Stolzenburg, M., and T. C. Marshall, 1994: Testing models of thunderstorm charge distributions with Coulomb's law. *J. Geophys. Res.,* **99** (D12), 25 921–25 932.

——, ——, W. D. Rust, E. C. Bruning, D. R. MacGorman, and T. Hamlin, 2007: Electric field values observed near lightning flash initiations. *Geophys. Res. Lett.,* **34,** L04804, doi:10.1029/2006GL028777.

Takahashi, T., 1978: Riming electrification as a charge generation mechanism in thunderstorms. *J. Atmos. Sci.,* **35,** 1536–1548.

Tessendorf, S. A., L. J. Miller, K. C. Wiens, and S. A. Rutledge, 2005: The 29 June 2000 supercell observed during STEPS. Part I: Kinematics and microphysics. *J. Atmos. Sci.,* **62,** 4127–4150.

——, S. A. Rutledge, and K. C. Wiens, 2007: Radar and lightning observations of normal and inverted polarity multicellular storms from STEPS. *Mon. Wea. Rev.,* **135,** 3682–3706.

Thomas, R. J., P. R. Krehbiel, W. Rison, S. J. Hunyady, W. P. Winn, T. Hamlin, and J. Harlin, 2004: Accuracy of the lightning mapping array. *J. Geophys. Res.,* **109,** D14207, doi:10.1029/2004JD004549.

Wang, P. K., and H. R. Pruppacher, 1977: Acceleration to terminal velocity of cloud and raindrops. *J. Appl. Meteor.,* **16,** 275–280.

Weinheimer, A. J., 1987: The electrostatic energy of a thunderstorm and its rate of change. *J. Geophys. Res.,* **92** (D8), 9715–9722.

Weiss, S. A., D. R. MacGorman, and K. M. Calhoun, 2012: Lightning in the anvils of supercell thunderstorms. *Mon. Wea. Rev.,* **140,** 2064–2079.

Wiens, K. C., S. A. Rutledge, and S. A. Tessendorf, 2005: The 29 June 2000 supercell observed during STEPS. Part II: Lightning and charge structure. *J. Atmos. Sci.,* **62,** 4151–4177.

Williams, E. R., 1985: Large-scale charge separation in thunderclouds. *J. Geophys. Res.,* **90** (D4), 6013–6025.

——, and R. M. Lhermitte, 1983: Radar tests of the precipitation hypothesis for thunderstorm electrification. *J. Geophys. Res.,* **88** (C15), 10 984–10 992.

——, C. M. Cooke, and K. A. Wright, 1985: Electrical discharge propagation in and around space charge clouds. *J. Geophys. Res.,* **90** (D4), 6059–6070.